Int. J. Sci. R. Tech., 2026 3(4)
A Multidisciplinary peer-reviewed Journal
www.ijsrtjournal.com [ISSN: 2394-7063]

Original Article

Plant-Mediated Green Synthesis, Characterization And Applications Of Cr_2O_3 And Mgo Nanoparticles

A. Nancy*, Antony Rajam

PG Department of Chemistry, St. Mary's College (Autonomous) Thoothukudi - 628001.

ABSTRACT

This study reports the green synthesis of chromium oxide (Cr_2O_3) and magnesium oxide (MgO) nanoparticles using *Alpinia officinarum* leaf extract as a reducing and stabilizing agent. Characterization by UV–Visible, FT-IR, XRD, FE-SEM, EDAX, and TGA confirmed nanoparticle formation, crystallinity, and thermal stability. UV spectra showed peaks at 266 and 353 nm for Cr_2O_3 and ~270 nm for MgO, while XRD indicated well-defined crystalline structures at the nanoscale. FT-IR analysis revealed phytochemical involvement in nanoparticle capping. Morphological studies showed agglomerated Cr_2O_3 and clustered MgO nanoparticles. Both nanoparticles exhibited antibacterial and anticorrosion properties, with MgO demonstrating superior antimicrobial activity and better corrosion resistance in neutral and basic media, while Cr_2O_3 performed better in acidic conditions. Additionally, *Alpinia officinarum* extract improved fruit shelf life by reducing microbial spoilage. Overall, MgO nanoparticles showed greater potential for sustainable biomedical and industrial applications.

Keywords: Green synthesis, Cr_2O_3 and MgO nanoparticles, Antibacterial activity, Corrosion inhibition, Alpinia officinarum extract

INTRODUCTION

Alpinia officinarum, a medicinal rhizomatous herb of the Zingiberaceae family, contrasts significantly with inorganic materials such as chromium and magnesium oxide in origin, composition, and applications.[5] While *A. officinarum* is rich in diverse bioactive phytochemicals including flavonoids, diarylheptanoids, and phenylpropanoids conferring antioxidant, antimicrobial, and reproductive health benefits, chromium is a transition metal primarily valued for its physicochemical properties such as high hardness, corrosion resistance, and multiple oxidation states (+2, +3, +6), enabling its extensive use in metallurgy, electroplating, and pigments.[4,3,6] In contrast, magnesium oxide (MgO), a thermally stable inorganic compound with a cubic crystal structure, exhibits strong basicity, high melting point, and notable biocompatibility, making it suitable for applications in refractory materials, medicine, and nanotechnology. Importantly, both *A. officinarum* and MgO share emerging relevance in green nanotechnology,[1,2] where plant-derived phytochemicals and MgO nanoparticles demonstrate significant antimicrobial and anticancer activities. Additionally, *A. officinarum* shows protective effects against oxidative stress and chemotherapy-induced toxicity, whereas chromium compounds, particularly in higher oxidation states, may exhibit toxicological concerns despite their industrial importance. Overall, this comparison highlights the distinction between a bioactive medicinal plant and inorganic materials while emphasizing their converging roles in advanced biomedical and nanotechnological applications.[7]

MATERIALS & METHODS

a. Collection of plants

The *Alpinia officinarum* plant was collected from the Municipal Corporation Nursery in Thoothukudi during the month of July. The leaves were separated from the plant, thoroughly washed with double distilled water to remove surface impurities and dried in the dark at room temperature for approximately 15 days.

b. Preparation of Leaf Extract

The leaves were smashed into a coarse powder using a blender. The leaf powder was stored in a dry, airtight

Relevant conflicts of interest/financial disclosures: The authors declare that the research was conducted in the absence of any commercial or financial relationships that could be construed as a potential conflict of interest.

container away from direct sunlight. About 5 g of dry powder was mixed with 100 mL of double distilled water and kept in a magnetic stirrer for 45 minutes. The herbal extraction was cooled to 37°C before being filtered using Whatman filter paper. The purified leaf extract was stored at 4°C for further nanoparticle (NP) synthesis.

c. Synthesis of Cr_2O_3 Nanoparticles

A clear solution containing 40 mL of plant extract and 0.2 M chromium chloride salt solution was placed in a 250 mL beaker. Three drops of NaOH were added and the mixture was magnetically stirred for 1 hour at 100°C. The formation of nanoparticles (NPs) was monitored by observing the color change of the solution. After allowing the solution to cool, the formed Cr_2O_3 nanoparticles were collected and dried in an oven at 80°C. The dried nanoparticles were then collected for further characterization and applications. The synthesized Cr_2O_3 nanoparticles prepared using *Alpinia officinarum* leaf extract were designated as throughout the study.

d. Synthesis of MgO Nanocomposite

To 40 mL of *Alpinia officinarum* leaf extract, 10 mL of 0.1 M $Mg(NO_3)_2$ solution was added and the mixture was stirred continuously for 45 minutes. Subsequently, 6.0 mL of 0.2 M NaOH was added dropwise to the mixture to form a visible precipitate. After the addition of NaOH, a color change from dark yellow to light yellow was observed. The mixture was then aged overnight. After aging, the solution was kept in an oven at 150°C for 4 hours until it dried and formed a powder. The obtained powder was then annealed at 500°C for 2 hours and collected for further characterization and applications.

RESULTS AND DISCUSSION

a. UV -Visible analysis

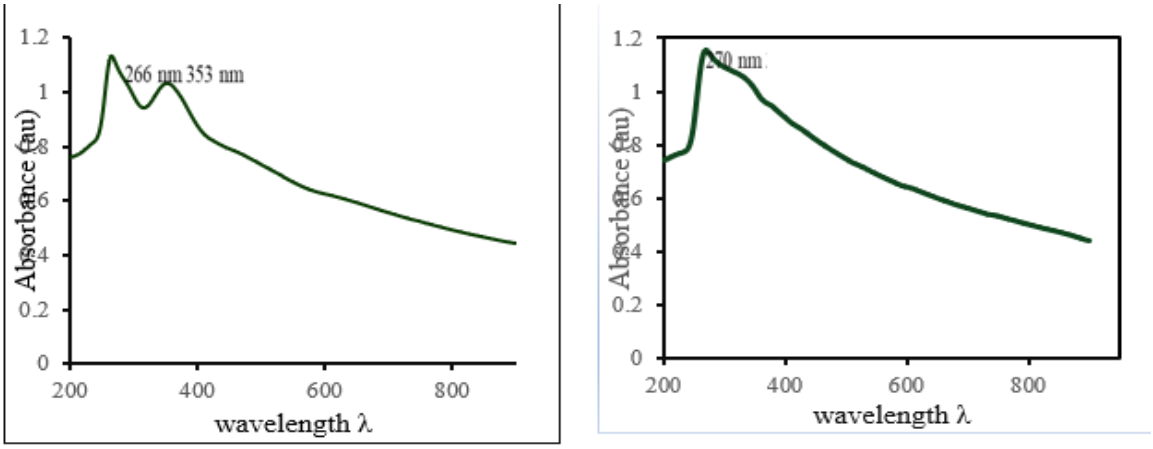


Figure 1: UV-Vis spectrum of a) Cr_2O_3 nanoparticles, b) MgO nanoparticles

The UV–Visible absorption spectra of chromium oxide (Cr_2O_3) and magnesium oxide (MgO) nanoparticles reveal comparable optical characteristics, with both materials exhibiting strong absorption bands in the ultraviolet region at approximately 266 nm and ~270 nm, respectively, attributed to intrinsic electronic transitions. In both cases, the absorbance markedly decreases beyond 400 nm, indicating negligible interaction within the visible region and suggesting their potential applicability in UV-based optical systems. Notably, Cr_2O_3 nanoparticles exhibit an additional absorption band around 353 nm, reflecting more complex electronic transitions, whereas MgO nanoparticles display a relatively simple spectral profile with a single dominant absorption peak. These observations confirm the successful synthesis of nanoscale materials, with MgO nanoparticles (10–40 nm) demonstrating a sharper and more defined absorption feature compared to the broader spectral response observed for Cr_2O_3 nanoparticles [8,14].

b. FT-IR Analysis

The FT-IR spectra of green-synthesized chromium oxide (Cr_2O_3) and magnesium oxide (MgO) nanoparticles, recorded in the range of 4000–400 cm^{-1}, exhibit several common features that confirm the role of biomolecules in nanoparticle formation and stabilization. In both spectra, a broad absorption band around ~3395–3396 cm^{-1} corresponds to O–H

stretching vibrations, while bands near ~2920 cm^{-1} are attributed to aliphatic C–H stretching, indicating the presence of organic residues from the plant extract. Additional peaks observed in the regions ~1600–1700 cm^{-1} and ~1000–1100 cm^{-1} in both materials are associated with carbonyl (C=O), aromatic (C=C), and C–O/C–O–C functional groups, suggesting the involvement of phytochemicals as reducing and capping agents. However, a distinct band at ~552 cm^{-1} in Cr_2O_3 nanoparticles corresponds to Cr–O–Cr stretching, confirming the formation of chromium oxide nanostructures, whereas MgO nanoparticles are characterized by metal–oxygen bonding in the lower wavenumber region without a similarly prominent isolated peak. Overall, the FT-IR analysis confirms the successful synthesis of both nanomaterials and highlights the presence of surface-bound biofunctional groups, with Cr_2O_3 showing more defined metal–oxygen vibrational features and MgO exhibiting a broader range of organic functional group interactions [9,15].

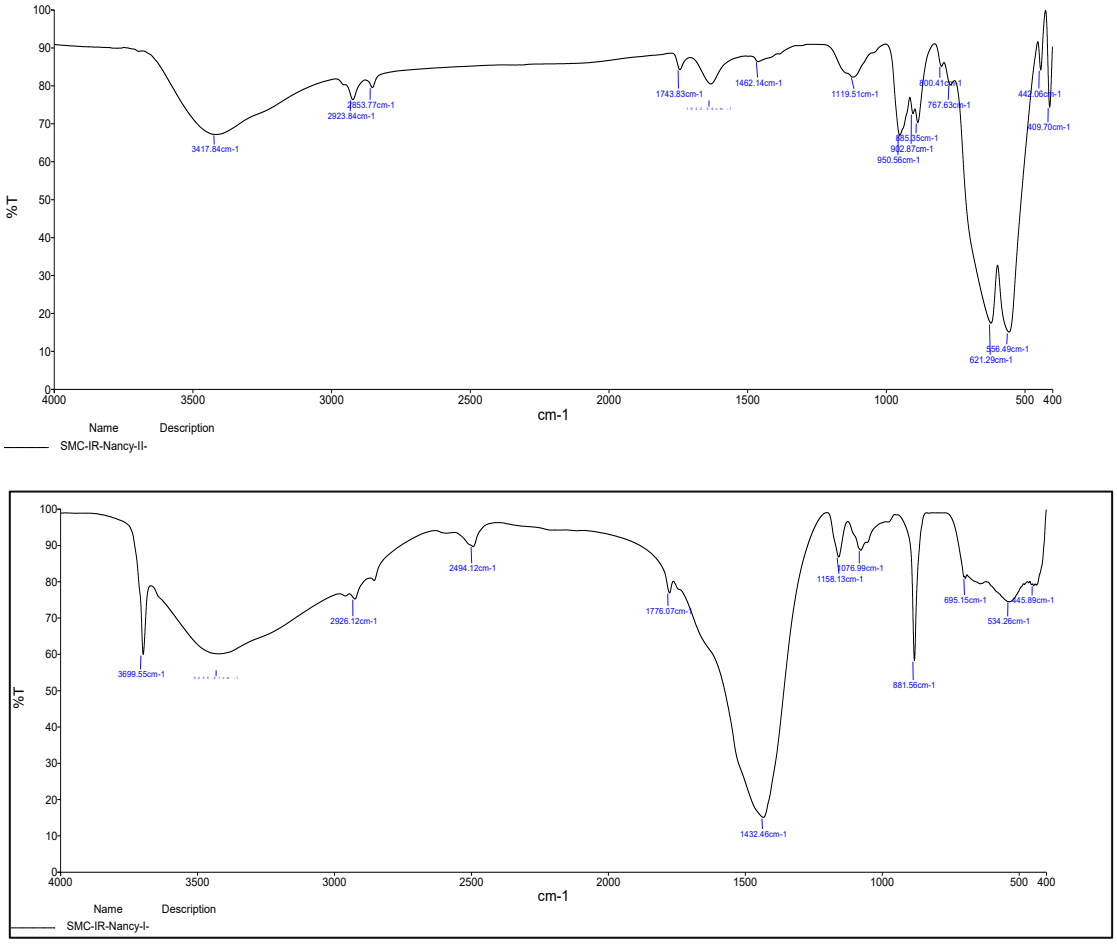


Figure 2: FT-IR Spectrum of a) Cr_2O_3 nanoparticles, b) MgO nanoparticles

c. X-RAY Diffraction Studies The X-ray diffraction (XRD) patterns of the synthesized chromium oxide (Cr_2O_3) and magnesium oxide (MgO) nanoparticles confirm their crystalline nature and successful formation at the nanoscale. In both cases, well-defined and sharp diffraction peaks were observed, indicating high crystallinity and phase purity. The crystallite sizes, calculated using the Debye–Scherrer equation, with Cr_2O_3 exhibiting an average size of ~28 nm and MgO showing a smaller size of ~13.1 nm. However, distinct differences in crystal structure were evident: Cr_2O_3 nanoparticles displayed a rhombohedral phase with characteristic reflections corresponding to planes such as (012), (104), and (110), whereas MgO nanoparticles exhibited a cubic crystal structure with diffraction peaks indexed to planes including (111), (002), and (222). Additionally, the prominent

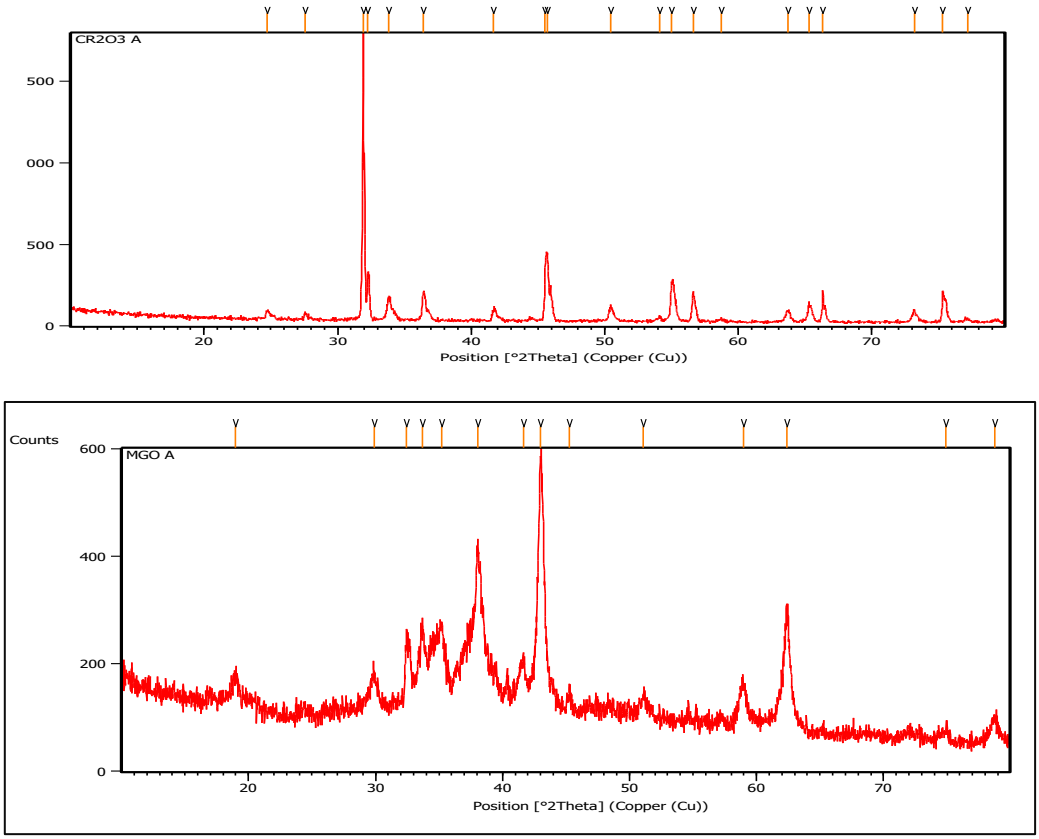
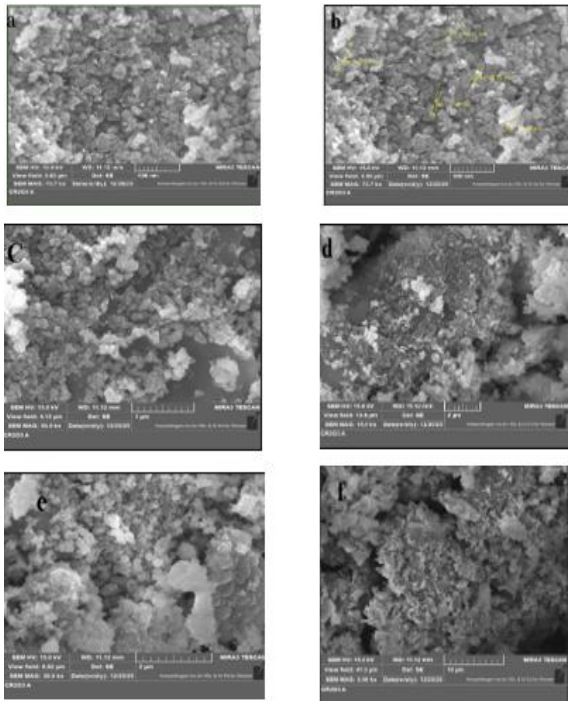


Figure 3: XRD spectrum of a) Cr_2O_3 nanoparticles, b) MgO nanoparticles

(104) peak in Cr_2O_3 suggests preferential orientation, while MgO demonstrates a polycrystalline nature with uniformly distributed peaks.

d. Field Emission Scanning Electron Microscopy (FESEM)

Field Emission Scanning Electron Microscopy (FE-SEM) analysis of the synthesized chromium oxide (Cr_2O_3) and magnesium oxide (MgO) nanoparticles reveals notable similarities in their surface morphology, with both materials exhibiting predominantly quasi-spherical particle shapes and significant agglomeration. In both cases, the particles form large aggregated clusters, with sizes ranging from approximately 500 nm to 10 µm and an average particle size of ~5.25 µm, indicating strong interparticle interactions during the synthesis process. However, MgO nanoparticles display a more distinct cauliflower-like clustered morphology with a relatively rough surface texture, as observed across multiple magnifications, whereas Cr_2O_3 nanoparticles exhibit a comparatively granular morphology with less pronounced structural complexity. These observations confirm that both nanomaterials are composed of aggregated nanoscale units forming microscale clusters, with MgO showing more defined surface structuring and Cr_2O_3 presenting a simpler granular appearance [11,17].



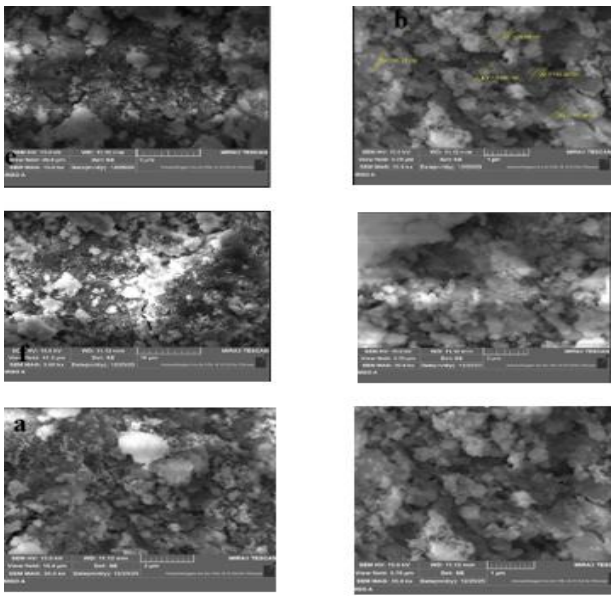


Figure 4: FESEM images of Cr_2O_3 nanoparticles in different magnification a) 500nm b)500nm c) 1µm d) 2µm e) 2µm f) 10µm MgO nanoparticles in different magnification a) 2µm b) 1µm c) 1µm d) 1µm e) 5µm f) 10µm

e. EDAX ANALYSIS

Energy Dispersive X-ray (EDAX) analysis of the synthesized chromium oxide (Cr_2O_3) and magnesium oxide (MgO) nanoparticles confirms that both materials are predominantly composed of their respective metal and oxygen elements, demonstrating successful formation and high purity. In both cases, the major elements (Cr and O for Cr_2O_3; Mg and O for MgO) exhibit significant weight and atomic percentages consistent with their expected stoichiometry, while minor trace elements such as sodium and other impurities are present in small amounts without contributing to secondary phase formation. Elemental mapping for both nanomaterials reveals a uniform distribution of the principal elements, indicating homogeneous composition and effective synthesis. However, Cr_2O_3 nanoparticles show relatively higher metal weight contribution compared to oxygen, whereas MgO nanoparticles display a more balanced elemental ratio between Mg and O. Additionally, MgO contains a slightly broader range of trace elements (Na, K, Ca) compared to Cr_2O_3 (Na, Cl). Overall, the EDAX results validate the successful synthesis of well-dispersed, high-purity nanostructures for both materials, with consistent elemental distribution and minimal impurity interference [12,19]

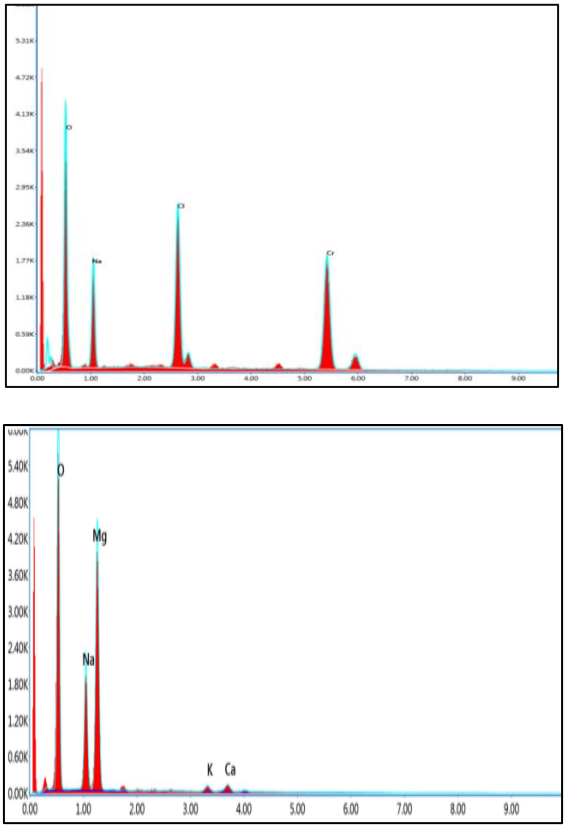


Figure 5: EDAX spectrum of a) Cr_2O_3 nanoparticles, b) MgO nanoparticles

f. Thermogravimetric Analysis (TGA)

Thermogravimetric analysis (TGA) of the synthesized chromium oxide (Cr_2O_3) and magnesium oxide (MgO) nanoparticles demonstrates distinct thermal behaviors while confirming the stability of both materials at elevated temperatures. In both cases, an initial weight loss at lower temperatures is attributed to the removal of physically adsorbed moisture and surface-bound volatile species, followed by further weight reduction due to the decomposition of residual organic compounds originating from the synthesis process. However, Cr_2O_3 nanoparticles exhibit significantly higher thermal stability, with minimal total weight loss (less than ~5%) up to 1000 °C, indicating a robust and stable crystalline framework. In contrast, MgO nanoparticles display a more pronounced multi-step weight loss, particularly in the 250–500 °C range, associated with substantial decomposition of organic residues and intermediate degradation processes. Additionally, MgO shows continued weight reduction at higher temperatures, reflecting secondary decomposition and residue oxidation, whereas Cr_2O_3 undergoes only minor changes, suggesting structural stabilization. Overall,

while both nanomaterials retain their inorganic frameworks at high temperatures, Cr_2O_3 demonstrates superior thermal stability compared to MgO, making it more suitable for demanding high-temperature applications [13,18]

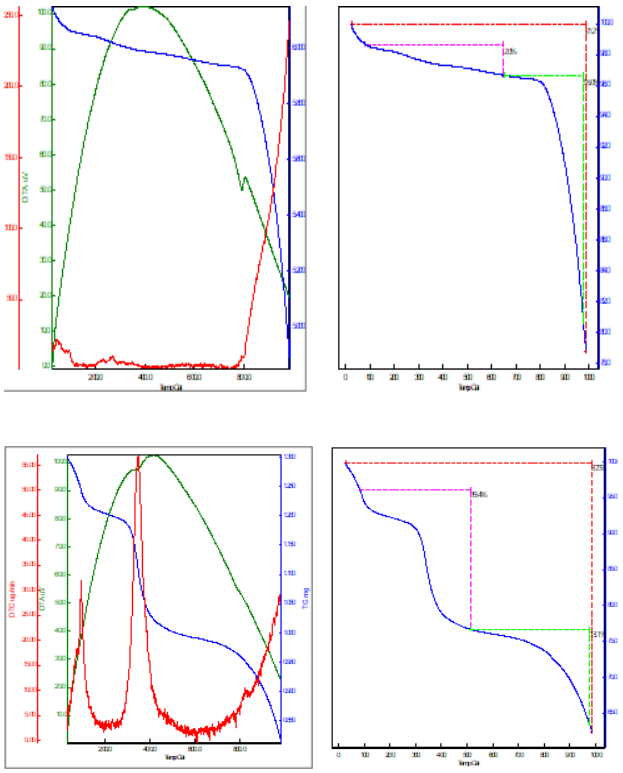


Figure 6: TGA of the synthesized a) Cr_2O_3 nanoparticles, b) MgO nanoparticles

Table 1: Elemental composition of Cr_2O_3 and MgO nanoparticles

Sample	Element	Weight %	Atomic %
Cr_2O_3	O K	45.12	60.84
	Na K	5.21	4.88
	Mg K	46.37	32.54
	45.12	60.84	0.97
	Ca K	1.54	0.77
	O K	45.12	60.84
MgO	Na K	5.21	4.88
	Mg K	46.37	32.54
	K K	1.76	0.97
	Ca K	1.54	0.77
	O K	45.12	60.84

g. Antibacterial activity

The antibacterial potential of chromium oxide (Cr_2O_3) and magnesium oxide (MgO) nanoparticles was evaluated using the disc diffusion method against Gram-positive (*Staphylococcus aureus*, *Bacillus subtilis*, *Bacillus cereus*) and Gram-negative (*Escherichia coli*, *Klebsiella pneumoniae*) bacteria, with ciprofloxacin as a standard control. Both nanoparticles exhibited measurable zones of inhibition, confirming their antimicrobial activity, though with varying efficacy. Comparative analysis revealed that MgO nanoparticles displayed superior antibacterial activity relative to Cr_2O_3. MgO showed the highest inhibition against *Bacillus cereus* (15 mm) and *Klebsiella pneumoniae* (14 mm), whereas Cr_2O_3 demonstrated comparatively lower activity across all tested strains (Table 5.9). The enhanced activity of MgO is likely due to its higher surface reactivity, generation of reactive oxygen species (ROS), and stronger interaction with bacterial cell membranes. In contrast, the relatively inert oxide structure of Cr_2O_3 and lower ROS production may account for its reduced antibacterial performance. Despite both nanoparticles showing lower activity than ciprofloxacin, the presence of distinct inhibition zones confirms their antimicrobial potential. Overall, MgO nanoparticles exhibited more consistent and pronounced antibacterial effects compared to Cr_2O_3, highlighting their suitability for applications requiring antimicrobial functionality.

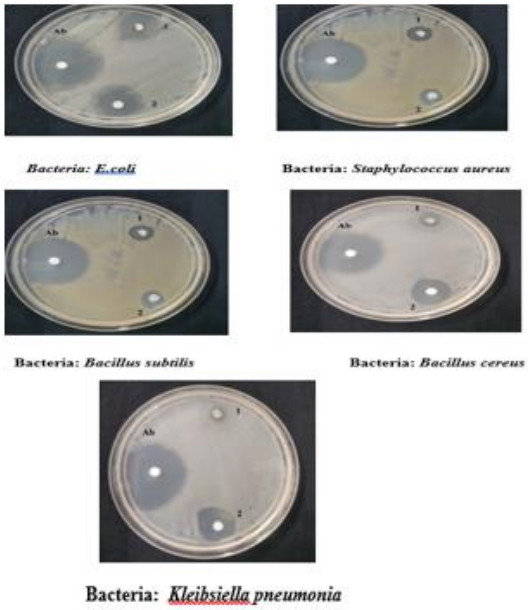


Figure 7: Antibacterial activity of Cr_2O_3 and MgO nano in a) *E.coli* b) *Staphylococcus aureus* c) *Bacillus subtilis* d) *Bacillus cereus* e) *Kleibsiella pneumonia*

Table 2: Antibacterial activity of Cr_2O_3 and MgO nanoparticles

Bacteria	Inhibition zone in mm		
	Ab ciprofloxacin	1-Cr2O3	2-MgO
E.coli	23	7	9
Staphylococcus aureus	25	9	10
Bacillus subtilis	26	7	8
Bacillus cereus	23	7	15
Kleibsiella pneumonia	25	6	14

h. Anticorrosion Activity

The anticorrosion performance of chromium oxide (Cr_2O_3) and magnesium oxide (MgO) nanoparticles was systematically evaluated in acidic, basic, and neutral media. Both nanoparticle treatments significantly reduced the corrosion rate of the metal substrate relative to untreated samples, demonstrating their protective capability. In acidic medium, Cr_2O_3 and MgO exhibited anti-corrosion efficiencies of 40.85% and 22.23%, respectively, whereas in basic medium, the efficiencies were 11.62% for Cr_2O_3 and 60.00% for MgO. In neutral medium, the protective effect increased, with efficiencies of 41.30% for Cr_2O_3 and 73.31% for MgO. The observed reduction in corrosion is attributed to the formation of a stable barrier layer that limits direct contact between the corrosive environment and the metal surface. Notably, corrosion rates were lowest under neutral conditions, indicating greater stability of the nanoparticle coatings, while acidic and basic media induced comparatively higher corrosion due to their aggressive nature.

Comparative analysis reveals that MgO-treated samples consistently outperformed Cr_2O_3-treated samples across all media, likely due to enhanced surface coverage, higher surface reactivity, and the formation of a more uniform protective layer. Cr_2O_3 nanoparticles also contributed to corrosion resistance through passive oxide layer formation, although their effectiveness was lower under identical conditions. Overall, both Cr_2O_3 and MgO nanoparticle coatings improved the corrosion resistance of the metal substrate, with MgO demonstrating superior performance (Tables 5.10–5.12; Figures 5.20–5.22).

Table 3: Anti-correction activity of acidic medium

Medium	**Wi**	**Wf**	**ΔW**	**Percentage %**	**Anti-correction activity in percentage**
Blank	7.7789	7.5075	0.2714	3.48	-
Cr2O3	7.6636	7.5982	0.0654	0.85	75
MgO	7.7540	7.5808	0.1732	2.23	34

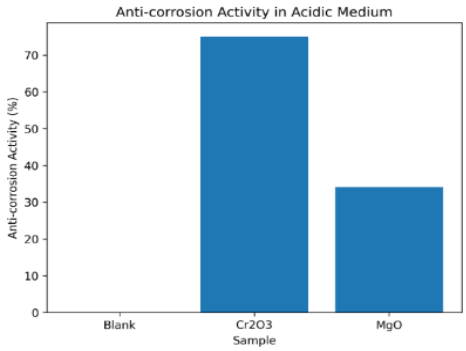


Figure 8 Anticorrosion Activity of Cr2O3 and MgO Nanoparticle in acidic medium

Table 4: Anti-correction activity of acidic medium

Medium	Wi	Wf	ΔW	Percentage %	Anti-correction activity in percentage
Blank	7.6630	7.4717	0.1913	2.49	-
Cr2O3	7.7010	7.5759	0.1251	1.62	35
MgO	7.8062	7.4932	0.3130	4.00	60

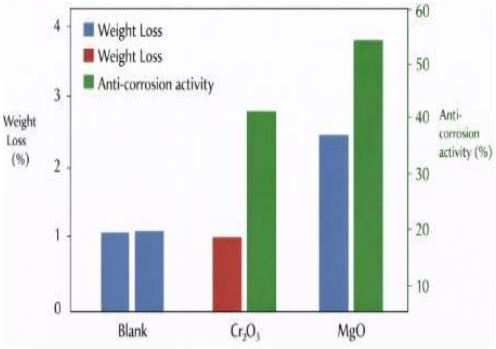


Figure 9 Anticorrosion Activity of Cr2O3 and MgO Nanoparticle in basic medium

Table 5 Anti-correction activity of Neutral

Medium	Wi	Wf	ΔW	Percentage %	Anti-correction activity in percentage
Blank	7.6476	7.6545	0.0069	0.09	-
Cr2O3	7.7045	7.6041	0.1004	1.30	13
MgO	7.6551	7.6264	0.0287	0.37	31

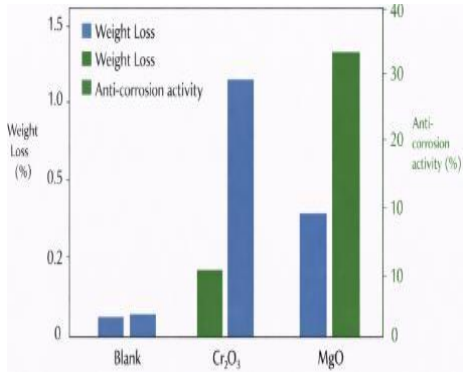


Figure 10 Anticorrosion Activity of Cr2O3 and MgO Nanoparticle in neutral

CONCLUSION

Cr_2O_3 and MgO nanoparticles were successfully synthesized via a green route using Alpinia officinarum leaf extract as a reducing and stabilizing agent. The nanoparticles were thoroughly characterized by UV–Visible spectroscopy, FT-IR, XRD, FE-SEM, EDAX, and thermogravimetric analysis (TGA), confirming their formation, crystallinity, morphology, and thermal stability. UV–Visible spectra revealed strong absorption peaks at 266 nm and 353 nm for Cr_2O_3 and around 270 nm for MgO, indicating pronounced UV absorption and suitability for optical applications. FT-IR analysis confirmed the presence of functional groups from phytochemicals involved in nanoparticle capping, while metal–oxygen vibrations (Cr–O–Cr at ~552 cm^{-1} and Mg–O for MgO) verified successful nanoparticle formation. XRD patterns indicated hexagonal Cr_2O_3 and cubic MgO crystalline phases with average crystallite sizes of ~2.01 nm and ~2.23 nm, respectively. FE-SEM images showed granular, agglomerated Cr_2O_3 nanoparticles and quasi-spherical, clustered MgO particles, consistent with EDAX elemental analysis, which confirmed major constituents as Cr/O and Mg/O, respectively.
TGA analysis demonstrated good thermal stability for both nanoparticles, with major degradation stages observed at ~750°C for Cr_2O_3 and 350–400°C for MgO, while residual mass at higher temperatures confirmed structural integrity. Antibacterial activity assessed against five pathogenic strains (Escherichia coli, Staphylococcus aureus, Bacillus subtilis, Bacillus cereus, and Klebsiella pneumoniae) revealed measurable inhibition zones for both nanoparticles, with MgO exhibiting superior activity (maximum inhibition: Bacillus cereus 15 mm, Klebsiella pneumoniae 14 mm). Food preservation studies further indicated that Alpinia officinarum extract coatings enhanced the shelf life of fruits and vegetables by reducing microbial growth, moisture loss, and oxidative deterioration.

In addition, anti-corrosion testing on mild steel demonstrated that both Cr_2O_3 and MgO nanoparticle coatings effectively reduced corrosion rates across acidic, basic, and neutral media. Cr_2O_3 showed better performance in acidic conditions, whereas MgO offered higher corrosion protection under neutral and basic conditions, highlighting their potential as eco-friendly protective coatings. Overall, the comparative study confirmed that MgO nanoparticles, in particular, exhibit superior crystallinity, thermal stability, antibacterial activity, corrosion resistance, and food preservation capability. These findings suggest that green-synthesized Cr_2O_3 and MgO nanoparticles are promising multifunctional materials for sustainable applications in catalysis, biomedical, environmental, and industrial protection.

REFERENCES

1. Sawai J, Kojima H, Igarashi H, Hasimoto A, Shoji S, Sawaki T et al. Antibacterial characteristics of magnesium oxide powder. World Journal of Microbiology and Biotechnology. 2000; 16:187-194.
2. Ganapathi Rao K, Ashok CH, Venkateshwara Rao K, Shilpa Chakra CH, Akshay Kranth A. Structural properties of MgO NPs, synthesized by Co-precipitation technique. International Journal of Adv. Research in Physical Science, ISSN (online) 2013; 2319-7064.
3. Sourav Saha, Gouranga Dutta, et. al. (2025) Sustainable synthesis of Cr2O3 nanoparticles utilizing Rauvolfiatetraphylla root extract for lung cancer treatment Journal of Drug Delivery Science and Technology Volume 104, 106531 https://doi.org/10.1016/j.jddst.2024.10653
4. Muhammad Mohsin Altaf, Han Yi, et. al. (2024) Mitigating chromium stress in tomato plants using green-silicone nanoparticles: Enhancing cellular oxidative stress management and chromium reduction Scientia Horticulture Volume 338, 113635 https://doi.org/10.1016/j.scienta.2024.113635.
5. Kose LP, Gulcin I, Goren AC, et al. LC–MS/MS analysis, antioxidant and anticholinergic properties of galanga (Alpinia officinarum Hance) rhizomes. Industrial Crops and Products. 2015; 74:712–721.
6. Ghalehkandi, G.J. (2014): Garlic (Allium sativum) juice protects from semen oxidative stress in male rats exposed to chromium chloride. Anim. repro'd; 11,4;526- 532.
7. Iyer, A., et al. (2010). Antioxidant and antimicrobial activity of Alpinia officinarum 11:767-771.
8. Iqbal, J.; Munir, A.; Uddin, S. Facile green synthesis approach for the production of

chromium oxide nanoparticles and their different in vitro biological activities. Microsc. Res. Tech. 2020, 83, 706–719.
9. Ahmed Mohamed, H.E.; Afridi, S.; Khalil, A.T.; Zohra, T.; Ali, M.; Alam, M.M.; Ikram, A.; Shinwari, Z.K.; Maaza, M. Phyto-fabricated Cr2O3 nanoparticle for multifunctional biomedical applications. Nanomedicine 2020, 15, 1653–1669.
10. Khan, S.A.; Shahid, S.; Lee, C.-S. Green Synthesis of Gold and Silver Nanoparticles Using Leaf Extract of Clerodendrum inerme; Characterization, Antimicrobial, and Antioxidant Activities. Biomolecules 2020, 10, 835.
11. Khan, S.A.; Shahid, S.; Shahid, B.; Fatima, U.; Abbasi, S.A. Green Synthesis of MnO Nanoparticles Using Abutilon indicum Leaf Extract for Biological, Photocatalytic, and Adsorption Activities. Biomolecules 2020, 10, 785.
12. Ahmad, Z.; Shamim, A.; Mahmood, S.; Mahmood, T. Biological synthesis and characterization of chromium (iii) oxide nanoparticles. Eng. Appl. Sci. Lett. 2018, 1, 23–29
13. Chen, L.; Song, Z.; Wang, X.; Prikhodko, S.V.; Hu, J.; Kodambaka, S.; Richards, R. Three-dimensional morphology control during wet chemical synthesis of porous chromium oxide spheres. ACS Appl. Mater. Interfaces 2009, 1, 1931–1937
14. Jorfi, S. et al. Enhanced coagulation-photocatalytic treatment of Acid red 73 dye and real textile wastewater using UVA/synthesized MgO nanoparticles. J. Environ. Manag. 177, 111–118 (2016).
15. 1Dekermenjian, M., Ruediger, A. P. & Merlen, A. Raman spectroscopy investigation of magnesium oxide nanoparticles. RSC Adv. 13(38), 26683–26689 (2023)
16. Rezaei, M., Khajenoori, M. & Nematollahi, B. Synthesis of high surface area nanocrystalline MgO by pluronic P123 triblock copolymer surfactant. Powder Technol. 205(1), 112–116 (2011).
17. Noha, A. K. et al. Renin and angiotensin converting enzyme inhibition of standardized bioactive fractions of Hyphaene thebaica L mart growing in Egypt. Pharm. J. 10(4), 622 (2018).
18. Pugazhendhi, A. et al. Anticancer, antimicrobial and photocatalytic activities of green synthesized magnesium oxide nanoparticles (MgONPs) using aqueous extract of Sargassum wightii. J. Photochem. Photobiol. B: Biol. 190, 86–97 (2019).
19. Dobrucka, R. Synthesis of MgO nanoparticles using Artemisia abrotanum Herba Extract and their antioxidant and photocatalytic properties. Iran. J. Sci. Technol.Trans. A Sci. 42(2), 547–555 (2018).

HOW TO CITE: A. Nancy*, Antony Rajam, Plant-Mediated Green Synthesis, Characterization And Applications Of Cr2O3 And Mgo Nanoparticles, Int. J. Sci. R. Tech., 2026, 3 (4), 827-836. https://doi.org/10.5281/zenodo.19698205